This is an open access article published under an ACS AuthorChoice License, which permits copying and redistribution of the article or any adaptations for non-commercial purposes.

cm CHEMISTRY OF MATERIALS

Communication

pubs.acs.org/cm

Highly Scalable Synthesis of MoS_2 Thin Films with Precise Thickness Control via Polymer-Assisted Deposition

Heeseung Yang,[†,#] Anupam Giri,[‡,#] Sungmin Moon,[‡] Sangbae Shin,[‡] Jae-Min Myoung,[*,†] and Unyong Jeong[*,‡]

[†]Department of Materials Science Engineering, Yonsei University, 134 Shinchon-dong, Seoul, Korea

[‡]Department of Materials Science and Engineering, Pohang University of Science and Technology, 77 Cheongam-Ro, Nam-Gu, Pohang 790-784, Korea

Supporting Information

Downloaded by POHANG UNIV OF SCIENCE & TECHNOLOGY at 22:13:02:377 on June 13, 2019 from https://pubs.acs.org/doi/10.1021/acs.chemmater.7b01605.

Transition metal dichalcogenides (TMDs) have been receiving intensive attention because of their potential use in a wide range of applications. Molybdenum disulfide (MoS_2) thin films, in particular, have found unique uses in catalysis,[1] sensor,[2] piezoelectricity,[3] electrical energy storage,[4] hydrogen storage,[5] optoelectronics, and transistors.[6,7] In addition, the tunability of the large intrinsic bandgap (1.2−1.8 eV) and the high mechanical flexibility of MoS_2 thin films facilitate its use as a semiconductor for flexible electronic devices.[8] These versatile applications demand large-scale synthesis of MoS_2 thin films with high uniformity in thickness and composition. Significant efforts have been devoted to preparing MoS_2 thin films, including mechanical exfoliation with scotch tape,[9] chemical exfoliation in a liquid phase and coating,[10] chemical vapor deposition (CVD),[11,12] and hydrothermal synthesis and coating.[13,14] Although the CVD process has been successfully used to produce high-quality MoS_2 thin films, it is limited with respect to low-cost synthesis and scale-up for massive production.[8,15,16] Coating a solution phase ink on a substrate cannot provide an ultrathin film with uniform thickness over large area. In terms of cost and scalability, a two-step synthesis including the solution-based coating of a precursor and then the formation of a MoS_2 thin film would be an advantageous alternative. Recently, the polymer-assisted deposition (PAD) has been used successfully to generate uniform metal oxide thin films.[17,18] In PAD, a polymer is used to stabilize the charged metal precursor and enables uniform coating of the polymer−precursor complex. Even though the PAD approach is immediately applicable to the synthesis of two-dimensional thin films, it has been limited to the synthesis of metal oxide thin films.

There are several challenging issues in the two-step film formation on a target substrate. Ideally, the synthesis of MoS_2 thin films should (i) be a scalable process with high uniformity in thickness and chemical composition, (ii) allow precise control of the thickness, (iii) not require a supply of additional sulfur during the synthesis, (iv) enable low-temperature synthesis, and (v) result in a product with high crystal quality. So far, only a few reports have been published for MoS_2 thin films.[19−21] Lie et al. synthesized a highly crystalline centimeter-scale MoS_2 thin film by dip-coating a precursor solution onto an insulating substrate.[13] The precursor film was converted into MoS_2 via a two-step thermolysis (at 500 and 1000 °C) with a flux of sulfur. Lee et al. exploited the self-assembly of precursor molecules into long lines during the dip-coating process using high-temperature thermolysis with a sulfur flux to produce MoS_2 wires.[22] Lim et al. coated a precursor dissolved in ethylene glycol onto various substrates and then converted the precursor into MoS_2 at a relatively low temperature (450 °C).[23] Kwon et al. reported the synthesis of a MoS_2 thin-film catalyst for the hydrogen evolution reaction. They used a two-step annealing process, with the first step at 500 °C under flowing N_2 and H_2 and the second step at 900 °C under a reducing ambient atmosphere without an additional sulfur source.[24] A few more studies involving similar procedures for the synthesis of MoS_2 thin films on Si wafers have also been published.[25−27]

The two-step approach developed thus far shares a common concept: coating a pure precursor onto a substrate and decomposing it at a high temperature to form a MoS_2 thin film. A precursor solution without including other materials is used to prevent possible contamination of the product thin film. However, such precursor solutions dewet readily on most substrates; this obstructs the formation of uniform precursor thin films and precludes precise control of the thickness. Scale-up of the production is another difficulty associated with the use of such pure precursor solutions. Because sulfur evaporates during synthesis at high temperatures, a continuous supply of the sulfur source is typically used to maintain the stoichiometry of the product film. This sulfurization prevents the reproducible fabrication of thin films with the same performance because the elemental composition of the product cannot be controlled by manipulating the initial solution conditions. The synthesis of MoS_2 thin films requires the development of a reproducible, scalable process that guarantees the formation of uniform ultrathin films with precise thickness control.

In this study, we develop a highly scalable coating process by using the polymer-assisted deposition and apply thermolysis at a relatively low temperature (700 °C) without sulfurization. This process enables fine control of the precursor film, which leads to precise thickness control of the resulting MoS_2 film (≥2 nm). In addition, we demonstrate the fabrication of a MoS_2-based photodetector with a broad spectral response and excellent performance, as indicated by its fast response time (<1.0 ms).

Received: April 19, 2017
Revised: June 27, 2017
Published: June 27, 2017

© 2017 American Chemical Society

DOI: 10.1021/acs.chemmater.7b01605
Chem. Mater. 2017, 29, 5772−5776

Our strategy for the large-area synthesis of the MoS_2 films is described in Figure 1A. The synthesis included the formation of a precursor−polymer complex thin film comprising anhydrous ammonium tetrathiomolybdate (ATM) precursor and linear-poly(ethylenimine) (L-PEI). The choice of complexing polymer was the key. The complexing polymer plays as coating agent and precursor binder by ionic interaction. The polymer helps uniform coating over a large area without dewetting. L-PEI decomposes starting at a relatively low temperature of 170 °C and obtains complete thermolysis at relatively low temperature of about 400 °C without carbon residue.[28] ATM and L-PEI formed a complex in DMF by ionic interaction with molecules so that they were quickly aggregated in the solution phase (Supporting Information, Figure S1). The complexation between ATM and L-PEI was confirmed by the shift of the Raman signal from 407 to 432 cm^{-1} (Supporting Information, Figure S2). The peak shift comes from the change in the vibration mode between Mo and S atoms in ATM.[29] In order to keep the solution phase without aggregation, we added a small amount of ethanolamine in the complex aggregate solution to dissolve the aggregate in the solution. The binding between ATM and ethanolamine allowed only partial complexation between the ATM and L-PEI; hence, uniform coating of the complex film via conventional coating techniques was readily achieved over the entire area of the substrate. The thermolysis of the precursor complex film generated a MoS_2 thin film. The thermolysis was performed at 700 °C without an additional sulfur source under an inert environment comprising 4% H_2 and 96% Ar mixture gas. To prevent the formation of oxide contaminants in the as-synthesized MoS_2 thin films, the precursor complex films were kept under vacuum at room temperature for 30 min. The vacuum process was used to remove oxygens and water at a minimized level to prevent possible oxidation of the film during the heat treatment process and to help the conversion to MoS_2 without additional supply of the source. Then, the chamber was filled with inert gas and the temperature was increased to 700 °C within 10 min using a rapid thermal annealing system. The anhydrous ATM was converted into MoS_3 in the range of 120−260 °C and then transformed into 2H-MoS_2 above 400 °C.[30,31]

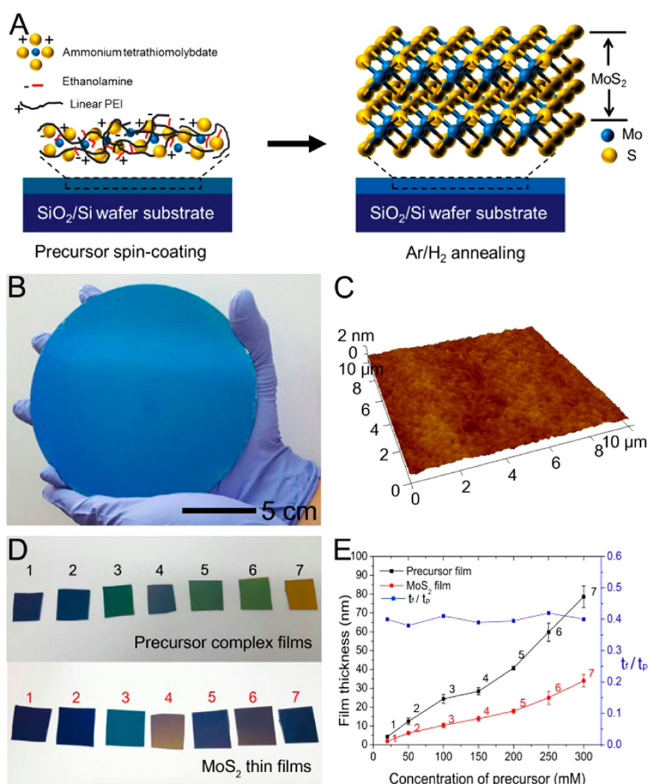

Figure 1. (A) Schematic illustration to form a polymer−precursor complex thin film and its conversion to a MoS_2 thin film on an SiO_2/Si wafer. (B,C) Digital image and three-dimensional AFM image of the as-synthesized MoS_2 thin film on a 6-in. SiO_2/Si wafer by spin-coating a 100 mM precursor solution. (D) Color changes by the thickness increase of the precursor complex films and the MoS_2 thin films. (E) Relationship between the film thickness and the precursor concentration in the complex solution. Black, red, and blue lines represent the thicknesses of the complex−precursor thin film (t_p) and the MoS_2 thin film (t_f) and their thickness ratio (t_f/t_p), resptectively.

Figure 1B shows a camera image of the MoS_2 thin film synthesized on a 6-in. Si wafer with a thick SiO_2 layer (300 nm) using the process described above. The uniform color over the whole area indicates the uniformity in the thickness of the film. The film thickness in the Figure was ∼9.1 nm (Supporting Information, Figure S3), and the average surface roughness of the film was less than 1 nm (Figure 1C). The thickness of the precursor complex film and consequently that of the MoS_2 thin film could be controlled by simply adjusting the concentration of the precursor in the coating solution. Figure 1D displays the color difference according to the film thicknesses of the precursor complex films and the MoS_2 films. Figure 1E shows the relationship between the precursor complex thickness and the MoS_2 film thickness. The MoS_2 thin films with controlled thicknesses (2−30 nm) were reproducibly prepared by spin-coating the precursor solutions with concentrations ranging from 20 mM to 300 mM. The spin-coating condition was fixed at 3000 rpm for 60 s in all the experiments. Notably, thicker films (e.g., 270 nm) could be prepared by bar-coating the precursor solution with a high precursor concentration (Supporting Information, Figure S4). The thickness ratio (t_f/t_p) between the precursor complex film (t_p) and the corresponding MoS_2 film thickness (t_f) was constant, i.e., on an average, $t_f = 0.39t_p$; this permitted precise control of the MoS_2 film thickness via adjusting the precursor concentration. The surface roughness increased with the thickness of the MoS_2 film (Supporting Information, Figure S5). The surface roughness of the precursor complex film governs the surface roughness of the MoS_2 film; therefore, careful coating of the precursor complex in a good coating facility can produce MoS_2 thin films with extreme flatness.

Figure 2 shows the transmission electron microscopy (TEM) images of the MoS_2 thin film shown in Figure 1B. The thin film was transferred to a TEM grid using the poly(methyl methacrylate) (PMMA)-based transfer method,[13] as described in the Supporting Information. Figure 2A shows a low-magnification TEM image, which shows the uniformity of the film over a large area. The fractures occurred during the transfer process. The high crystallinity of the thin film is evident from the high-resolution TEM (HR-TEM) image of the film (Figure 2B). The lattice distances of 0.274 and 0.161 nm match well the [100] and [110] planes of MoS_2, respectively. The selected-area electron diffraction (SAED) pattern in the inset image also confirms the hexagonal crystal structure of MoS_2. Figure 2C,D,E shows the cross-sectional HR-TEM images of MoS_2 films with different thicknesses. The thickness of MoS_2 film is controllable from about 2 nm to about 30 nm by spin coating.

DOI: 10.1021/acs.chemmater.7b01605
Chem. Mater. 2017, 29, 5772−5776

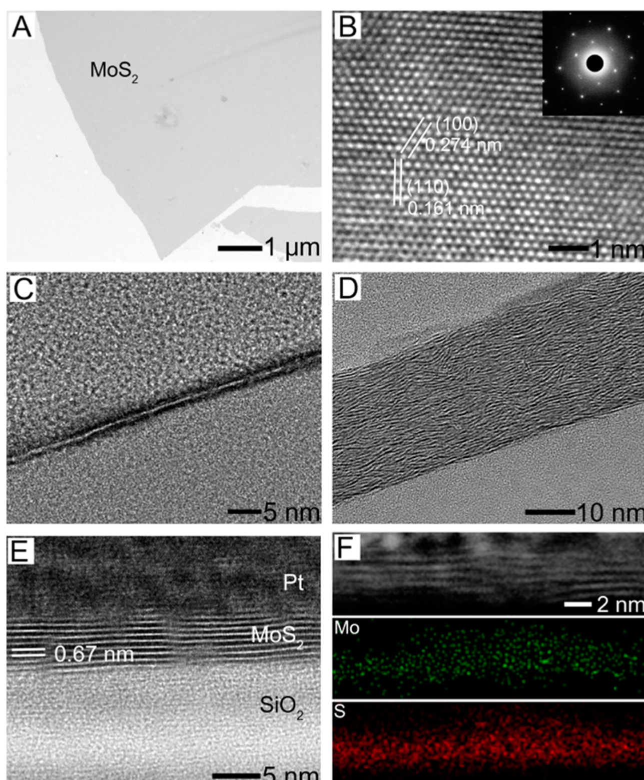

Figure 2. (A) Transmission electron microscope (TEM) image of the MoS_2 film (thickness = 9 nm) transferred onto a TEM grid. The cracks were formed during the transfer process. (B) High-resolution TEM image and diffraction pattern (in the inset) of the MoS_2 film. (C, D, and E) Cross-sectional TEM images of the MoS_2 films with different thicknesses. (E) STEM-HAADF image and elemental mapping of Mo (in green) and S (in red).

From Figure 2E, the interlayer distance and the thickness were determined to be 0.67 and 9 nm, respectively; the film was also found to comprise 13−14 layers aligned along the *c*-axis in Figure 2E. Figure 2F shows the images obtained using cross-sectional scanning TEM with high-angle annular dark-field (STEM-HAADF) and the results of the energy-dispersive X-ray spectroscopic (EDS) analysis of the Mo and S atoms. The atomic ratio was stoichiometric (Mo:S = 1:2) over the whole detection range, indicating the successful formation of an MoS_2 thin film. The grain size of synthesized MoS_2 film was about 13 nm which was measured from HR-TEM images (Supporting Information, Figure S6).

The as-synthesized thin film was analyzed via X-ray photoelectron spectroscopy (XPS) and Raman spectroscopy to assess the precise stoichiometry, detect trace amounts of any unreacted precursor, and determine the oxidation of the film. Figure 3A,B shows the XPS Mo 3d and S 2p spectra of the large-area MoS_2 film on the SiO_2/Si wafer. The Mo binding energies of 229.6 and 232.7 eV correspond to the Mo $3d_{5/2}$ and Mo $3d_{3/2}$ peaks, respectively. The S binding energies of 162.5 and 163.7 eV correspond to the S $2p_{3/2}$ and S $2p_{1/2}$ peaks, respectively. These binding energies match the reported values of the MoS_2 crystal.[32] The stoichiometric ratio of Mo and S was obtained by integrating the peak area of the XPS spectra, and the value was found to be Mo:S = 1:1.96. The positions of the E_{2g} and A_{1g} peaks for the in-plane and out-of-plane vibrational modes, respectively, are known to be dependent on the thickness of the MoS_2 thin film.[33] MoS_2 thin films grown by the solution process are considered to have Raman intensities lower than thin films grown by CVD because of their poor crystallinity. The Raman spectra of the as-synthesized MoS_2 films with various thicknesses are summarized in Figure 3C. The E_{2g} peak position gradually decreased from 383 to 380 cm^{-1}, and the A_{1g} peak position shifted from 402 to 404 cm^{-1} as the thickness of the as-synthesized MoS_2 film increased from 2 to 32 nm. The number of MoS_2 layers can be estimated from the difference between the E_{2g} and the A_{1g} Raman modes (Δk).[34,35] The value Δk = 22 cm^{-1} at 20 mM indicates a stacking of 2−3 MoS_2 layers; this is in good agreement with the 2 nm-thick film measured via atomic force microscopy (AFM). The photoluminescence (PL) spectra of the 2 nm-thick film has two peaks at around 660 nm (major) and 610 nm (minor), respectively. However, the PL intensity was significantly decreased with increasing thickness of MoS_2 films by bandgap change in Figure 3D.[10,36] Figure 3E shows the X-ray diffraction (XRD) pattern of the MoS_2 thin film prepared by bar-coating the 300-mM precursor solution (270 nm in thickness). All of the diffraction peaks are indexed to the 2H-MoS_2 symmetry (JCPDS 37-1492).[37] In particular, the detected major peaks are based on [100] family planes, indicating horizontal alignment of the MoS_2 layers within the thin film.

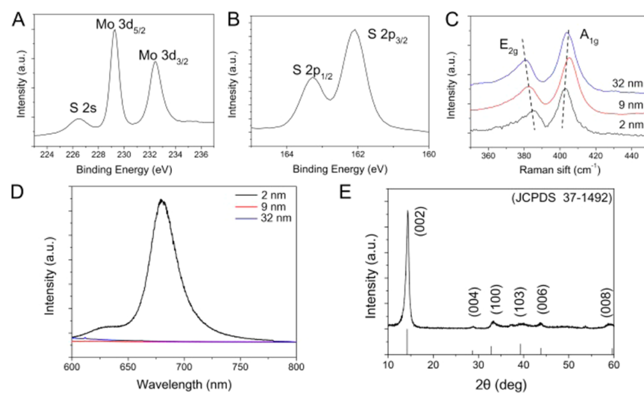

Figure 3. XPS spectra of the Mo 3d (A) and S 2p (B) binding energies of the MoS_2 films (thickness = 9 nm). (C) Raman spectra of the MoS_2 films with different thicknesses. (D) Photoluminescence spectra of the MoS_2 films with thickness variation. (E) XRD pattern of a MoS_2 film (thickness = 270 nm) prepared by bar-coating.

We used the as-synthesized MoS_2 thin films to fabricate sensitive photodetectors. To measure the photoelectrical properties of the thin films, we fabricated a two-probe photodetector without any gate bias (electrode channel length = 500 μm, active-layer area = 0.5 mm^2). Figure 4A shows the current (I)−voltage (V) characteristics of the photodetector fabricated using the 9 nm MoS_2 film. White light source was vertically projected onto the device under various illumination powers (30−140 μW). The current in the dark state was 8 nA at a 3 V bias voltage. The current increased to 1.47 μA at 30 μW and to 13.5 μA at 140 μW (on−off ratio = $\sim 10^4$). The responses to green (532 nm at 1 mW) and red lasers (633 nm at 1 mW) are shown in Supporting Information Figure S7. Figure 4B shows the dependence of the on−off ratios on the thickness of the MoS_2 thin films under the 532 nm green laser. The on−off ratio increased from $\sim 10^1$ to $\sim 10^4$ as the thickness of the MoS_2 film increased from 2 to 9 nm; it then decreased to $\sim 10^2$ at 32 nm (Supporting Information, Figure S8). On the basis of this result, the 9 nm-thick MoS_2 film was chosen as the photodetector active layer. The dependence of the on−off ratio

DOI: 10.1021/acs.chemmater.7b01605
Chem. Mater. 2017, 29, 5772−5776

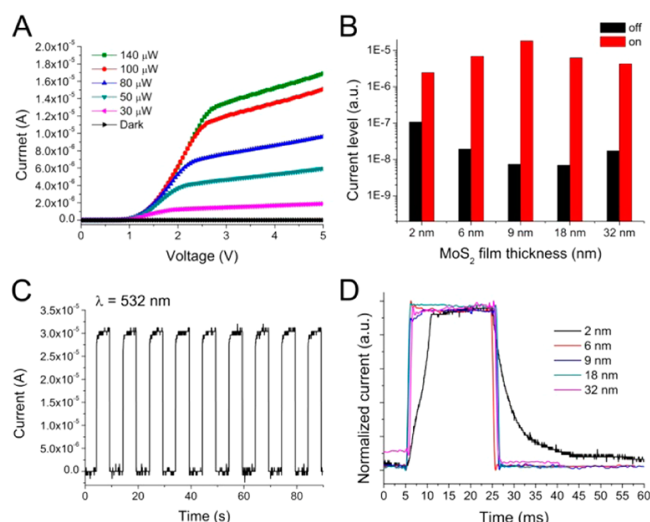

Figure 4. (A) Current (I)−voltage (V) characteristics of the photodetector in the dark and under different light illumination conditions (30−140 μW, 633 and 532 nm laser sources). (B) On−off ratio dependence on the film thicknesses. (C) Stability tests of the photoswitching behavior of the photodetector under the 532 nm laser illumination at 3 V. (D) Normalized photoresponse dependence on the MoS_2 film thickness.

on the film thickness is not clearly understood. In the crystal thin films prepared by CVD, the bandgap of the film decreases with increasing thickness,[38,39] so the off-current of the photodetector increases and the on−off ratio decreases. Clear understanding of the on−off ratio in this study requires several pieces of information: orientation and grain size of the crystals depending on the film thickness, interaction between the layers in the nanosized grains, and crystal structure and defects in the grain boundary. Those are critical information to predict the photoresponsivity of the film. The studies are left as our future task. The photoswitching behavior of the MoS_2 (9 nm in thickness) photodetector is shown in the time-resolved photocurrent response (Figure 4C). The green laser (532 nm, 1 mW) was irradiated at 3.0 V bias and turned on−off repeatedly with a periodicity of 10 s. The current sharply increased to 25 μA and then returned to 8 nA when the laser was turned on and off. Figure 4D shows the photocurrent responses of the MoS_2 films with various thicknesses in a higher time resolution. When the thickness was 2.0 nm, the response time (τ_r = 2 ms) and the decay time (τ_d = 4.5 ms) differed substantially. This substantial time difference between τ_r and τ_d might have originated from the presence of numerous defect states when the number of layers was small. However, when the thickness was larger than 6.0 nm, the photocurrent response was accomplished within 1.0 ms. This result can be attributed to a decrease in the defect density when the number of triple layers is larger than 10.

In summary, we successfully demonstrated a highly scalable two-step synthesis of MoS_2 thin films without sulfurization during the thermolysis step. Using a polymer that can form a complex with the precursor enabled precise control of the thickness (t_p) of the polymer−precursor complex films; this permitted quantitative control of the thickness (t_f) of the MoS_2 thin film ($t_f = 0.39t_p$, $t_f \geq 2$ nm) via adjustment in the precursor concentration. The synthesized MoS_2 film was uniform in thickness in a 6-in. wafer scale in this study. The photocurrent response of the as-synthesized MoS_2 films was dependent on the thickness of the film. When the film thickness was larger than 6 nm, the film exhibited a fast photoresponse (<1 ms), a high on−off ratio (~10^4) at low bias voltages, and highly stable reliability during repeated irradiation tests.

■ ASSOCIATED CONTENT

Supporting Information

The Supporting Information is available free of charge on the ACS Publications website at DOI: 10.1021/acs.chemmater.7b01605.

Experimental methods and Figures S1−S8 (PDF)

■ AUTHOR INFORMATION

Corresponding Authors

*(J.-M.M.) E-mail: jmmyoung@yonsei.ac.kr.

*(U.J.) E-mail: ujeong@postech.ac.kr.

ORCID

Jae-Min Myoung: 0000-0002-9895-4915

Unyong Jeong: 0000-0002-7519-7595

Author Contributions

[#]H.Y. and A.G contributed equally.

Author Contributions

H.Y. and A.G performed the experiments. S.S. contributed photocurrent characterization. S.M. performed TEM analysis. H.Y. wrote the manuscript. J.-M.M and U.J. designed the study and provided guidance. All authors discussed the results and commented on the manuscript at all stages.

Notes

The authors declare no competing financial interest.

■ ACKNOWLEDGMENTS

We are grateful for the financial support from the National Research Foundation of Korea (NRF) grant funded by the Korean Government (MSIP) under Project No. NRF-2015R1A2A1A10054164.

■ REFERENCES

(1) Voiry, D.; Salehi, M.; Silva, R.; Fujita, T.; Chen, M.; Asefa, T.; Shenoy, V. B.; Eda, G.; Chhowalla, M. Conducting MoS_2 Nanosheets as Catalysts for Hydrogen Evolution Reaction. *Nano Lett.* **2013**, *13*, 6222−6227.

(2) Cho, B.; Hahm, M. G.; Choi, M.; Yoon, J.; Kim, A. R.; Lee, Y. J.; Park, S. G.; Kwon, J. D.; Kim, C. S.; Song, M.; Jeong, Y.; Nam, K. S.; Lee, S.; Yoo, T. J.; Kang, C. G.; Lee, B. H.; Ko, H. C.; Ajayan, P. M.; Kim, D. H. Charge-transfer-based Gas Sensing Using Atomic-layer MoS_2. *Sci. Rep.* **2015**, *5*, 8052.

(3) Wu, W.; Wang, L.; Li, Y.; Zhang, F.; Lin, L.; Niu, S.; Chenet, D.; Zhang, X.; Hao, Y.; Heinz, T. F.; Hone, J.; Wang, Z. L. Piezoelectricity of single-atomic-layer MoS_2 for energy conversion and piezotronics. *Nature* **2014**, *514*, 470−474.

(4) Chang, K.; Chen, W. X. l-Cysteine-Assisted Synthesis of Layered MoS_2/Graphene Composites with Excellent Electrochemical Performances for Lithium Ion Batteries. *ACS Nano* **2011**, *5*, 4720−4728.

(5) Chen, J.; Kuriyama, N.; Yuan, H.; Takeshita, H. T.; Sakai, T. Electrochemical Hydrogen Storage in MoS_2 Nanotubes. *J. Am. Chem. Soc.* **2001**, *123*, 11813−11814.

(6) Huo, N.; Kang, J.; Wei, Z.; Li, S.-S.; Li, J.; Wei, S.-H. Novel and Enhanced Optoelectronic Performances of Multilayer MoS_2−WS_2 Heterostructure Transistors. *Adv. Funct. Mater.* **2014**, *24*, 7025−7031.

(7) Lopez-Sanchez, O.; Lembke, D.; Kayci, M.; Radenovic, A.; Kis, A. Ultrasensitive photodetectors based on monolayer MoS_2. *Nat. Nanotechnol.* **2013**, *8*, 497−501.

DOI: 10.1021/acs.chemmater.7b01605
Chem. Mater. 2017, 29, 5772−5776

(8) Ahn, C.; Lee, J.; Kim, H. U.; Bark, H.; Jeon, M.; Ryu, G. H.; Lee, Z.; Yeom, G. Y.; Kim, K.; Jung, J.; Kim, Y.; Lee, C.; Kim, T. Low-Temperature Synthesis of Large-Scale Molybdenum Disulfide Thin Films Directly on a Plastic Substrate Using Plasma-Enhanced Chemical Vapor Deposition. *Adv. Mater.* **2015**, *27*, 5223−5229.
(9) Li, H.; Wu, J.; Yin, Z.; Zhang, H. Preparation and Applications of Mechanically Exfoliated Single-Layer and Multilayer MoS_2 and WSe_2 Nanosheets. *Acc. Chem. Res.* **2014**, *47*, 1067−1075.
(10) Eda, G.; Yamaguchi, H.; Voiry, D.; Fujita, T.; Chen, M.; Chhowalla, M. Photoluminescence from Chemically Exfoliated MoS_2. *Nano Lett.* **2011**, *11*, 5111−5116.
(11) Samad, L.; Bladow, S. M.; Ding, Q.; Zhuo, J.; Jacobberger, R. M.; Arnold, M. S.; Jin, S. Layer-Controlled Chemical Vapor Deposition Growth of MoS_2 Vertical Heterostructures *via* van der Waals Epitaxy. *ACS Nano* **2016**, *10*, 7039−7046.
(12) Zhang, W.; Huang, J. K.; Chen, C. H.; Chang, Y. H.; Cheng, Y. J.; Li, L. J. High-Gain Phototransistors Based on a CVD MoS_2 Monolayer. *Adv. Mater.* **2013**, *25*, 3456−3461.
(13) Liu, K. K.; Zhang, W. J.; Lee, Y.-H.; Lin, Y.-C.; Chang, M.-T.; Su, C. − Y.; Chang, C.-S.; Li, H.; Shi, Y.; Zhang, H.; Lai, C.-S.; Li, L.-J. Growth of Large-Area and Highly Crystalline MoS_2 Thin Layers on Insulating Substrates. *Nano Lett.* **2012**, *12*, 1538−1544.
(14) Zhan, Y.; Liu, Z.; Najmaei, S.; Ajayan, P. M.; Lou, J. Large-Area Vapor-Phase Growth and Characterization of MoS_2 Atomic Layers on a SiO_2 Substrate. *Small* **2012**, *8*, 966−971.
(15) Choudhary, N.; Park, J.; Hwang, J. Y.; Choi, W. Growth of Large-Scale and Thickness-Modulated MoS_2 Nanosheets. *ACS Appl. Mater. Interfaces* **2014**, *6*, 21215−21222.
(16) Lee, G. − H.; Yu, Y. − J.; Cui, X.; Petrone, N.; Lee, C.-H.; Choi, M. S.; Lee, D. − Y.; Lee, C.; Yoo, W. J.; Watanabe, K.; Taniguchi, T.; Nuckolls, C.; Kim, P.; Hone, J. Flexible and Transparent MoS_2 Field-Effect Transistors on Hexagonal Boron Nitride-Graphene Heterostructures. *ACS Nano* **2013**, *7*, 7931−7936.
(17) Jia, Q. X.; Mccleskey, T. M.; Burrell, A. K.; Lin, Y.; Collis, G. E.; Wang, H.; Li, A. D. Q.; Foltyn, S. R. Polymer-Assisted Deposition of Metal-oxide Films. *Nat. Mater.* **2004**, *3*, 529−532.
(18) Yi, Q.; Wu, J.; Zhao, J.; Wang, H.; Hu, J.; Dai, X.; Zou, G. Tuning Bandgap of *p*-Type $Cu_2Zn(Sn, Ge)(S, Se)_4$ Semiconductor Thin Films via Aqueous Polymer-Assisted Deposition. *ACS Appl. Mater. Interfaces* **2017**, *9*, 1602−1608.
(19) Kong, D.; Wang, H.; Cha, J. J.; Pasta, M.; Koski, K. J.; Yao, J.; Cui, Y. Synthesis of MoS_2 and $MoSe_2$ Films with Vertically Aligned Layers. *Nano Lett.* **2013**, *13*, 1341−1347.
(20) Dumcenco, D.; Ovchinnikov, D.; Marinov, K.; Lazić, P.; Gibertini, M.; Marzari, N.; Sanchez, O. L.; Kung, Y.-C.; Krasnozhon, D.; Chen, M.-W.; Bertolazzi, S.; Gillet, P.; Fontcuberta i Morral, A.; Radenovic, A.; Kis, A. Large-Area Epitaxial Monolayer MoS_2. *ACS Nano* **2015**, *9*, 4611−4620.
(21) Han, G. H.; Kybert, N. J.; Naylor, C. H.; Lee, B. S.; Ping, J. L.; Park, J. H.; Kang, J.; Lee, S. Y.; Lee, Y. H.; Agarwal, R.; Johnson, A. T. C. Seeded Growth of Highly Crystalline Molybdenum Disulphide Monolayers at Controlled Locations. *Nat. Commun.* **2015**, *6*, 6128.
(22) Lee, S.-K.; Lee, J.-B.; Singh, J.; Rana, K.; Ahn, J. H. Drying-Mediated Self-Assembled Growth of Transition Metal Dichalcogenide Wires and their Heterostructures. *Adv. Mater.* **2015**, *27*, 4142−4149.
(23) Lim, Y. R.; Song, W.; Han, J. K.; Lee, Y. B.; Kim, S. J.; Myung, S.; Lee, S. S.; An, K.-S.; Choi, C.-J.; Lim, J. Wafer-Scale, Homogeneous MoS_2 Layers on Plastic Substrates for Flexible Visible-Light Photodetectors. *Adv. Mater.* **2016**, *28*, 5025−5030.
(24) Kwon, K. C.; Choi, S.; Hong, K.; Moon, C. W.; Shim, Y. S.; Kim, D. H.; Kim, T.; Sohn, W.; Jeon, J. M.; Lee, C.-H.; Nam, K. T.; Han, S.; Kim, S. Y.; Jang, H. W. Wafer-scale Transferable Molybdenum Disulfide Thin-film Catalysts for Photoelectrochemical Hydrogen Production. *Energy Environ. Sci.* **2016**, *9*, 2240−2248.
(25) Park, M.; Park, Y. J.; Chen, X.; Park, Y. K.; Kim, M.-S.; Ahn, J. H. MoS_2-Based Tactile Sensor for Electronic Skin Applications. *Adv. Mater.* **2016**, *28*, 2556−2562.
(26) Xi, Y.; Serna, M. I.; Cheng, L. X.; Gao, Y.; Baniasadi, M.; Rodriguez-Davila, R.; Kim, J.; Quevedo-Lopez, M. A.; Minary-Jolandan, M. Fabrication of MoS_2 Thin Film Transistors *via* Selective-area Solution Deposition Methods. *J. Mater. Chem. C* **2015**, *3*, 3842−3847.
(27) Giri, A.; Yang, H.; Thiyagarajan, K.; Jang, W.; Myoung, J. M.; Singh, R.; Soon, A.; Cho, K.; Jeong, U. One-Step Solution Phase Growth of Transition Metal Dichalcogenide Thin Films Directly on Solid Substrates. *Adv. Mater.* **2017**, 1700291.
(28) Kumar, C. S. S. *Nanostructured Thin Films and Surface*; Wiley-VCH: Weinheim, Germany, 2010.
(29) Lee, C.; Yan, H.; Brus, L. E.; Heinz, T. F.; Hone, J.; Ryu, S. Anomalous Lattice Vibrations of Single and Few-Layer MoS_2. *ACS Nano* **2010**, *4*, 2695−2700.
(30) Brito, J. L.; Ilija, M.; Hernandez, P. Thermal and Reductive Decomposition of Ammonium Thiomolybdates. *Thermochim. Acta* **1995**, *256*, 325−338.
(31) Walton, R. I.; Dent, A. J.; Hibble, S. J. In Situ Investigation of the Thermal Decomposition of Ammonium Tetrathiomolybdate Using Combined Time-Resolved X-ray Absorption Spectroscopy and X-ray Diffraction. *Chem. Mater.* **1998**, *10*, 3737−3745.
(32) Wang, X. S.; Feng, H. B.; Wu, Y. M.; Jiao, Y. L. Controlled Synthesis of Highly Crystalline MoS_2 Flakes by Chemical Vapor Deposition. *J. Am. Chem. Soc.* **2013**, *135*, 5304−5307.
(33) Kim, S. J.; Kang, M.-A.; Kim, S. H.; Lee, Y.; Song, W.; Myung, S.; Lee, S. S.; Lim, J.; An, K. − S. Large-scale Growth and Simultaneous Doping of Molybdenum Disulfide Nanosheets. *Sci. Rep.* **2016**, *6*, 24054.
(34) Lin, Y.-C.; Zhang, W. J.; Huang, J.-K.; Liu, K.-K.; Lee, Y.-H.; Liang, C.-T.; Chu, C.-W.; Li, L.-J. Wafer-scale MoS_2 thin layers prepared by MoO_3 sulfurization. *Nanoscale* **2012**, *4*, 6637−6641.
(35) Li, H.; Zhang, Q.; Yap, C. C. R.; Tay, B. K.; Edwin, T. H. T.; Olivier, A.; Baillargeat, D. From Bulk to Monolayer MoS_2: Evolution of Raman Scattering. *Adv. Funct. Mater.* **2012**, *22*, 1385−1390.
(36) Splendiani, A.; Sun, L.; Zhang, Y.; Li, T.; Kim, J.; Chim, C.-Y.; Galli, G.; Wang, F. Emerging Photoluminescence in Monolayer MoS_2. *Nano Lett.* **2010**, *10*, 1271−1275.
(37) Joensen, P.; Frindt, R. F.; Morrison, S. R. Single-layer MoS_2. *Mater. Res. Bull.* **1986**, *21*, 457−461.
(38) Huang, Y. L.; Chen, Y.; Zhang, W.; Quek, S. Y.; Chen, C.-H.; Li, L.-J.; Hsu, W. − T.; Chang, W. − H.; Zheng, Y. J.; Chen, W.; Wee, A. T. S. Bandgap Tunability at Single-layer Molybdenum Disulphide Grain Boundaries. *Nat. Commun.* **2015**, *6*, 6298.
(39) Kim, J. H.; Kim, T. H.; Lee, H.; Park, Y. R.; Choi, W.; Lee, C. J. Thickness-dependent Electron Mobility of Single and Few-layer MoS_2 Thin-film Transistors. *AIP Adv.* **2016**, *6*, 065106.

DOI: 10.1021/acs.chemmater.7b01605
Chem. Mater. 2017, 29, 5772−5776